NGU REPORT 2018.028

Gas flares in the Barents Sea, northeast of Kvitøya

GEOLOGY FOR SOCIETY

SINCE 1858

GEOLOGICAL SURVEY OF NORWAY

- NGU -

NORGES GEOLOGISKE UNDERSØKELSE
- NGU -

REPORT

Geological Survey of Norway
P.O.Box 6315 Torgarden
NO-7491 TRONDHEIM
Tel.: 47 73 90 40 00

Report no.: 2018.028
ISSN: 0800-3416 (print)
ISSN: 2387-3515 (online)
Grading: Open

Title:
Gas flares in the Barents Sea, northeast of Kvitøya

Authors:
Terje Thorsnes, Shyam Chand

Client:
NPD, NGU

County:

Commune:

Map-sheet name (M=1:250.000)

Map-sheet no. and -name (M=1:50.000)

Deposit name and grid-reference:

Number of pages:
Map enclosures:
Price (NOK): 95

Fieldwork carried out:	**Date of report:**	**Project no.:**	**Person responsible:**
2017, 2018	15.12.2018	311758	Reidun Bøe

Summary:

A total of 37 gas flares have been identified in a 325 km^2 area northeast of Kvitøya. Most of the flares occur in the western part of the area. Many occur along a NNW-SSE trend, indicating that they may be sourced from deep-seated NNW-SSE trending faults.

Sedimentary bedrock beneath a thin cover of soft sediments is indicated in a small depression in the western part of the study area, where we observe crag and tail structures and outcropping strata.

Very few pockmarks occur in the investigated area, and the pockmarks observed are small and shallow.

Keywords: Gas flares	Water column data	Multibeam echosounder
Backscatter	Gas flares	Pockmark
Outcropping bedrock	Faults	Sand waves

CONTENTS

1. INTRODUCTION

Marine methane vents and cold seeps are widespread on continental margins, including the Barents Sea (Skarke et al., 2014). Active seepage on the continental shelf is commonly associated with underlying oil and gas reservoirs, trapped gas under gas hydrates, and dissociation of gas hydrate (Milkov and Sassen, 2003). Detection of gas flares from marine methane vents and cold seeps can be efficiently detected using multibeam echosounders (Urban et al., 2017).

This study is from an area northeast of Kvitøya, where the Norwegian Petroleum Directorate (NPD) collected multibeam echosounder data in 2017 and 2018 in cooperation with the MAREANO programme (www.mareano.no). The data from these surveys have been processed and interpreted in order to identify natural gas seeps, visible as gas flares, in the water column data. The results from this interpretation will be available through the MAREANO gas flare database which will be published in 2019.

2. METHODS AND MATERIAL

The multibeam echosounder data were collected by FOSAE in a 325 km^2 area 30-50 km northeast of Kvitøya (figure 1) using a Kongsberg Maritime EM710 multibeam echosounder (MBE) system. The EM710 MBE is a 0.5x1.0 degrees system with an operating frequency of 70-100 kHz. The data set consist of two parts collected in 2017 (FOSAE-2017-Kvitoya) and in 2018 (FGMG-2018-Kvitoya). Maps of bathymetry and backscatter are presented in UTM36, WGS84.

The water column data were stored as separate WCD files in the Kongsberg EM710 system. The data were processed using standard parameters and converted to Fledermaus GWC format with highest resolution using Fledermaus Midwater (FMM). FMM was also used for visualizing the converted data to identify gas flare related anomalies in the water column. Qimera was used for extracting positions of individual gas bubbles and picking out the base of flares (either seen directly in the nadir region or projected in the off- nadir region.

During interpretation, the following procedure was used:

- The depth range was adjusted in order to maximise the vertical display of the line (FMM)
- The display was adjusted to 1:1 horizontal display (FMM)
- The colour range was adjusted to the dynamic range of signals in the water column, optimizing the display of water column features (FMM)
- The data were inspected using the R-stack water column view, and the stacked fan water column view (FMM)

- QPS Qimera was used for extraction of XYZ for individual gas bubbles, and for extracting the position of the base for the gas flares
- Qimera and Fledermaus were used for 2D and 3D visualisation.

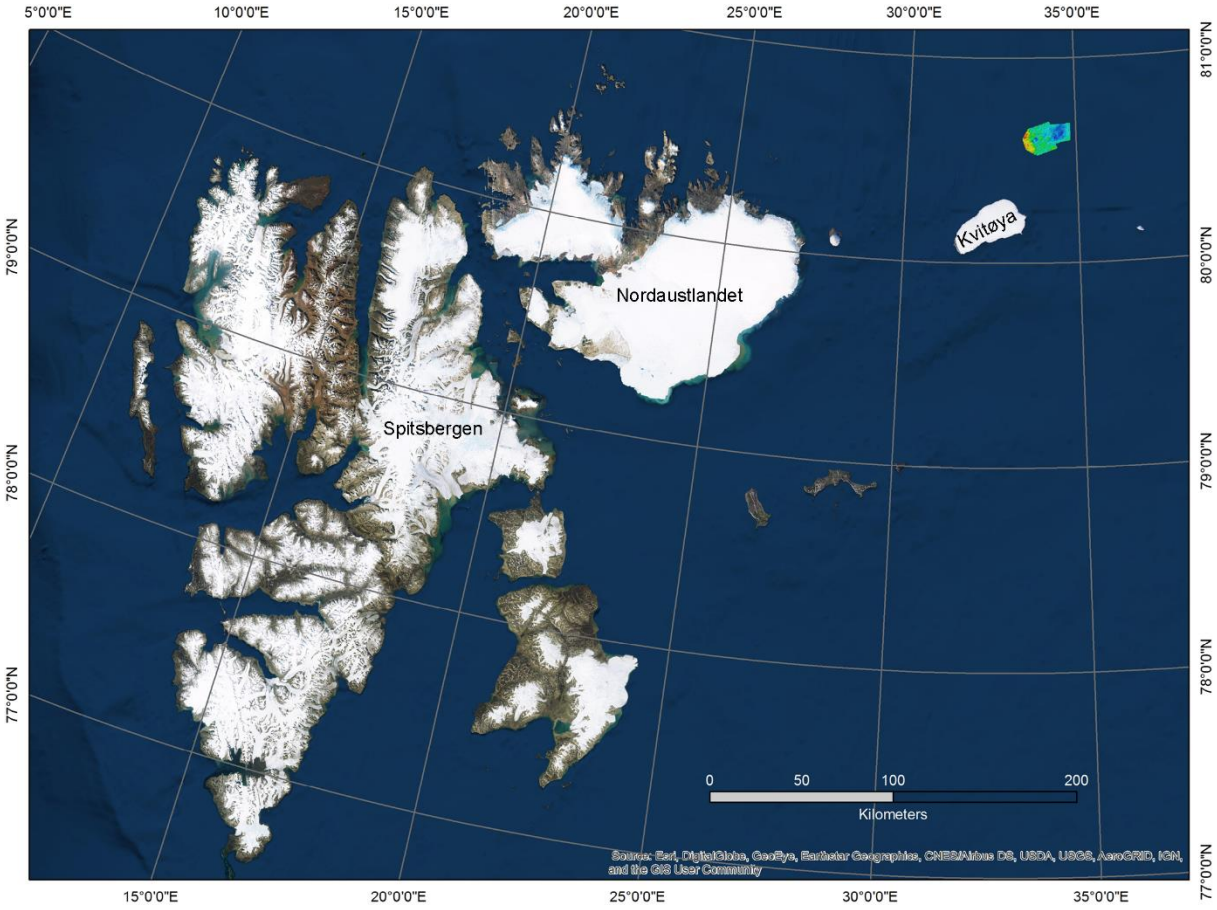

Figure 1. Overview map with Spitsbergen, Nordaustlandet and Kvitøya.

The water column data were evaluated in parallel (along-track) and perpendicular (across-track) directions to the track lines for identifying anomalies. The coordinates of potential gas flares were recorded, along with the survey name and line ID. A subjective assessment of the apparent magnitude has been assigned (table 1). A confidence estimate is provided for codes 2-6. The maximum confidence for visual classification is 90%. A confidence of 100% is reserved for gas flares where gas bubbles have been observed by video/photo inspection or measured using gas sniffers, or where authigenic carbonate crusts have been observed. Very uncertain, but still possible gas flares have been assigned 10% confidence (table 1). Generally, the recognition of gas flares is based on two criteria – the bubbles have higher backscatter strength than the ambient noise in the water column data, and the objects with higher backscatter strength form characteristic patterns in the water column. Under ideal conditions, gas plumes may be observed as flare-shaped objects which start at the seabed and become narrower until they disappear at least 50-100 m above the seabed. If currents are sufficiently strong, the flares will be deflected. The identification of gas flares may be complicated due to several factors, such as high ambient (periodic or random) noise, fish

schools, high density of plankton, strong and/or irregular currents, and sub-optimal intersection of the multibeam swath with the gas flare (i.e. covering only part of the flare).

Table 1. Codes used for assessment of magnitude, and confidence intervals.

Code	Description	Confidence %
2	Weak gas flare	10 - 100
3	Medium strong gas flare	10 - 100
4	Strong gas flare	10 - 100
5	Very strong gas flare	10 - 100
6	Giant gas flare	10 - 100

The interpretation of gas flares was locally challenging in the western part of the FOSAE-2017-Kvitoya area because of abundant biological material in the water column (plankton, fish, possibly some mammals). This may overprint wholly or partly the gas flares, or the biological material may form structures resembling gas flares (see examples in chapter 4 Results). There was little biological material observed in the FGMG-2018-Kvitoya data set, but here rather strong noise (probably caused by some acoustic or electric interference) may have overprinted the acoustic signatures of small gas flares.

3. GEOLOGICAL SETTING

The northern Svalbard margin is a part of the Eurasian margin of the Arctic Ocean. The Cenozoic development of the margin began when seafloor spreading in the Eurasian basin started in the earliest Tertiary and caused the separation of the Lomonosov ridge from the Barents/Siberian shelves (Geissler and Jokat, 2004). The Kvitøya and Nordaustlandet region was exposed land area during the Jurassic with shallow basins surrounding these regions (Leith et al., 1992). The onshore geology of the area comprises Late Precambrian crystalline rocks (Hecla Hoek Formation) on northeastern Nordaustlandet and Kvitøya, with a transition to younger, flat-lying Middle Carboniferous to Lower Cretaceous sediments (Lauritzen and Ohta, 1984, Hogan et al., 2010). Based on stratigraphical provinces of overlying Quaternary sediments and seismic data, a southeastwards trend from older Hecla Hoek rocks through to younger Permian and Triassic-Lower Jurassic sandstones and limestones is inferred (Elverhøi and Lauritzen, 1984). The boundary between Hecla Hoek rocks and Upper Permian sediments is mapped at the bathymetric sill at the southern end of Kvitøya Trough (Hogan et al., 2010).

The Nordaustlandet margin consists of a smooth basement surface covered by a few hundred metres of Quaternary sediments with velocities of as much as 1.9 km/s, indicating compaction due to former ice sheets in the inner shelf (Geissler and Jokat, 2004). Most of the sediments are probably of Cenozoic age (Eiken, 1992). The sediment thickness increases to 3-3.5 km in the outer shelf associated with down faulted basement (Geissler and Jokat, 2004). The inner shelf sediments consist typically of prograding sequences typically found in northern

glaciated margins. Repeated advances and retreats of glaciers pushed large volumes of terrigenous sediments beyond the shelf break resulting in shelf progradation. The fjords and troughs, e.g. the Kvitøya trough, demarcate former drainage pathways of the Svalbard-Barents Ice Sheet (Ottesen et al., 2005). The erosion rate of streaming ice was probably partly controlled by the underlying bedrock (Hogan et al., 2010) and also by differences in ice streaming velocities related to basal temperatures during various glaciations (e.g. during LGM, Patton et al., 2016).

The seabed in the investigated area (figure 2) varies from c. 230 mbsl (below sea level) to 70 mbsl. The shallowest part is found in the northwest, in a hilly area with iceberg ploughmarks on top. Two depressions occur – a small depression in the western part, and a larger in the eastern part. Both depressions are characterised by low backscatter (darker colour), indicating that the top sediments are soft and fine grained (figure 3).

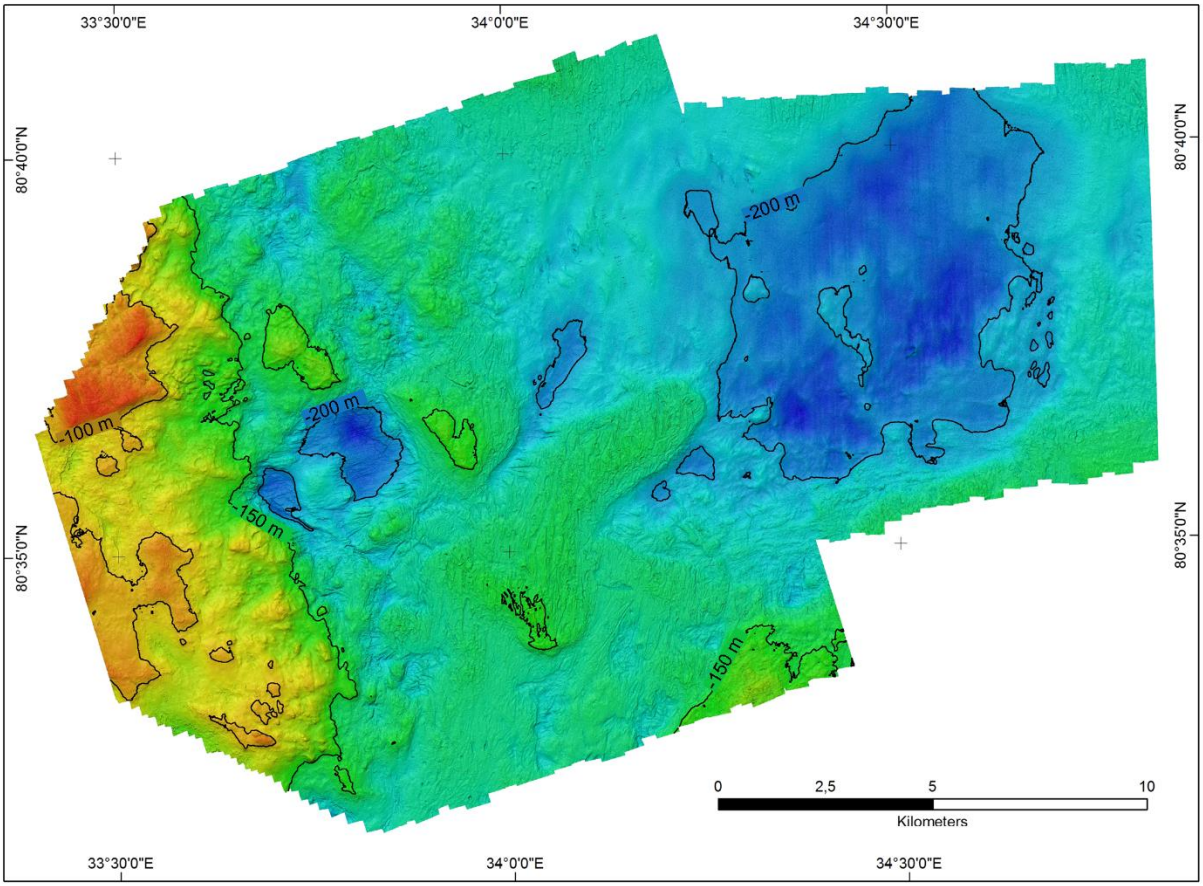

Figure 2. Bathymetry of the area northeast of Kvitøya.

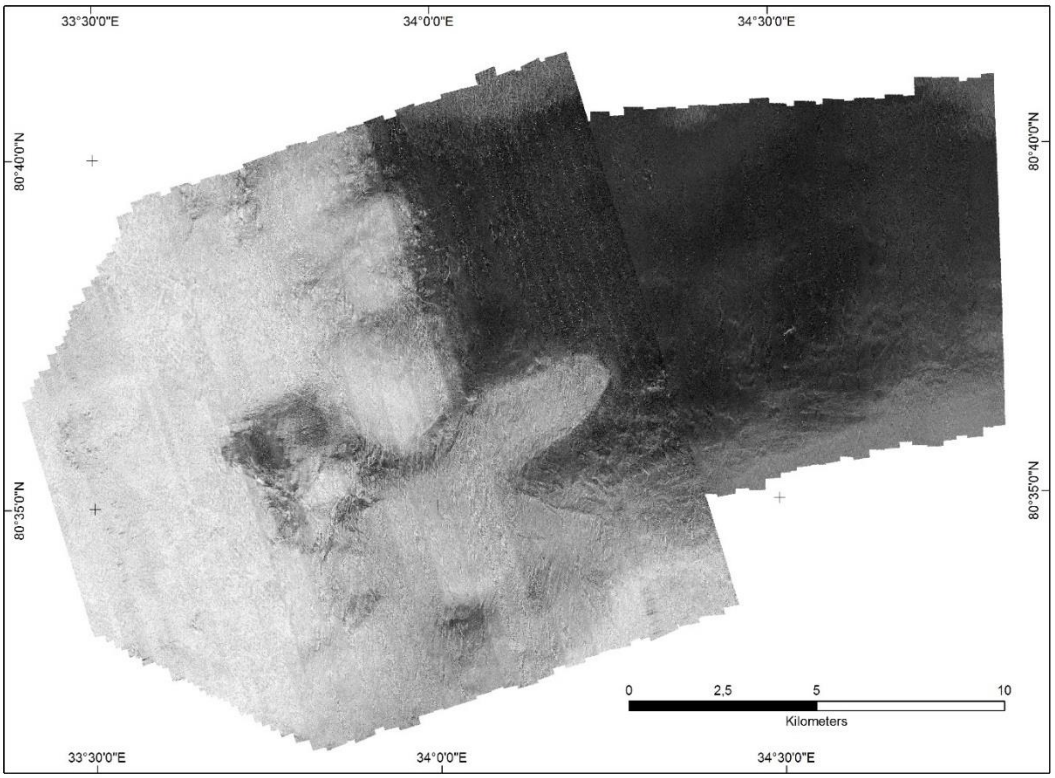

Figure 3. Backscatter of the area northeast of Kvitøya. UTM zone 36.

The small depression in the west is characterised by complex structures (figure 4). Arcuate ridges, pointing towards the ENE, are superimposed on ENE-WSW trending straight ridges. These straight ridges are locally asymmetrical and may form crag and tail structures. Terrace-like structures indicating erosion of bedding planes are found both in the southwest and in the central part of the depression (see inset figure). The crag and tail structures are interpreted to be formed by ice moving ENE over sedimentary bedrock, and the shape of the eroded bedding planes supports this interpretation. The origin of the arcuate ridges is uncertain. Eskers is one possibility, but other glacial processes should also be considered, taking into consideration that they generally point towards the ENE.

Sand waves up to 1 metre high are found in depressions in the central northern part of the study area, indicating relatively high current speeds (figure 5). Smaller sand waves are also found in the eastern depression, especially along the northern flank.

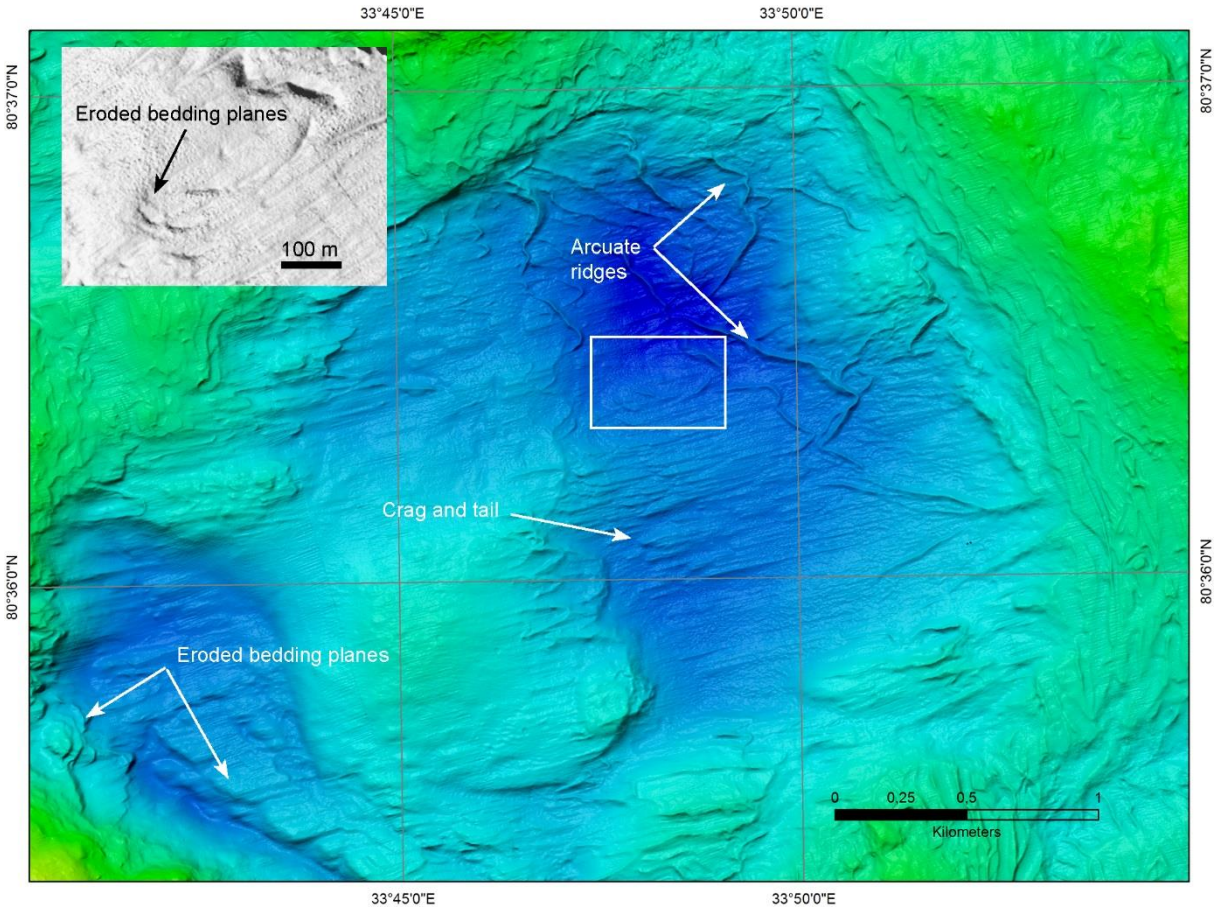

Figure 4. Complex structures in the western depression, with eroded bedding planes, crag and tail structures, and arcuate ridges. Water depth ranges from 225 metres (deep blue) til 150 metres (green).

Very few pockmarks have been observed, and those present are small – generally around 50 metres in diameter, and a few metres deep. They can be seen as small depressions in the bathymetry, and as higher reflectivity spots in the backscatter. Most of the pockmarks are found in the western depression (figure 6). The large depression in the east, with relatively soft sediments, has virtually no pockmarks. This contrasts with areas in the southern and central parts of the Barents Sea, where depressions filled with soft sediments may have thousands of pockmarks (Rise et al., 2015). No pockmarks have been observed associated with the gas flares. This may reflect a seabed dominated by till as indicated by high reflectivity and presence of iceberg plough marks (e.g. Rise et al., 2015).

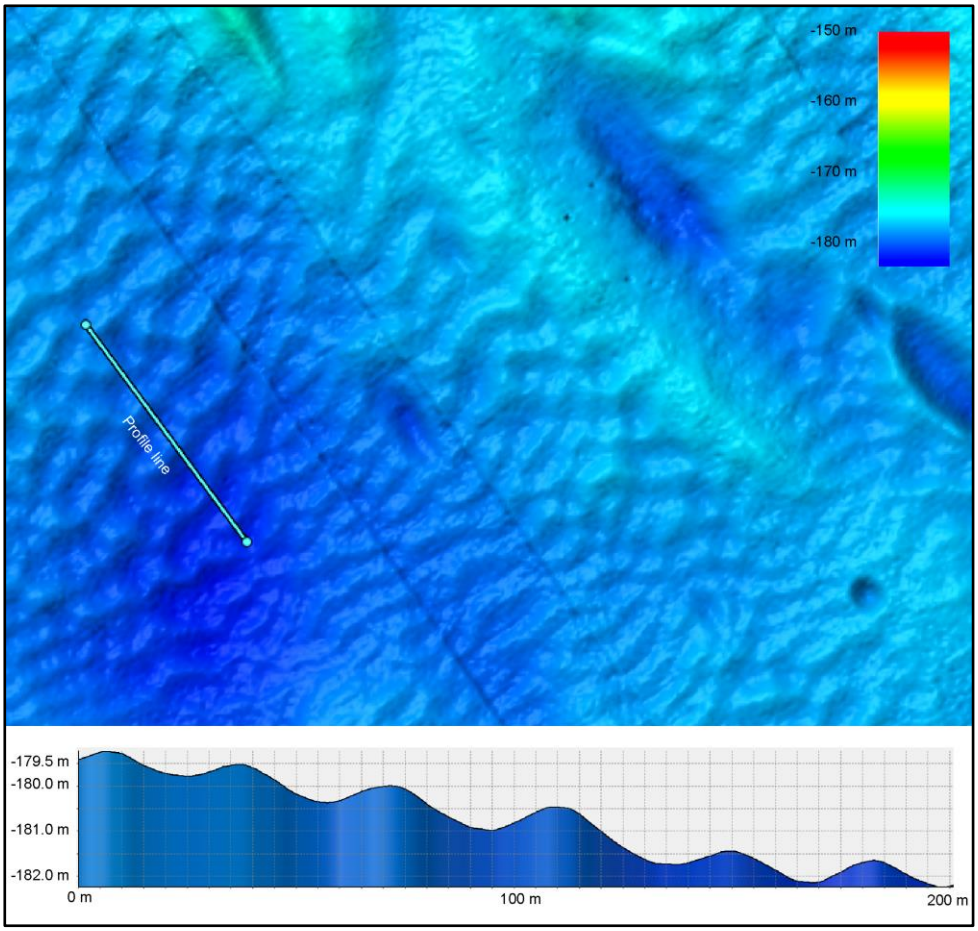

Figure 5. Sand waves in the central northern part of the study area.

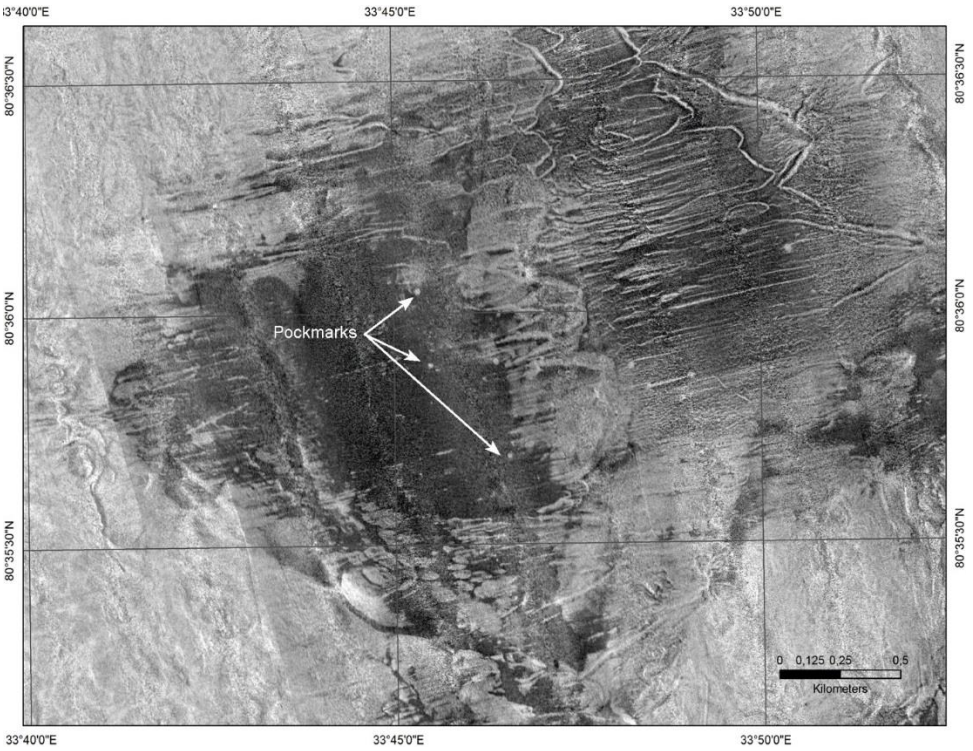

Figure 6. Pockmarks (white circles) in backscatter data.

Large sub-circular to elongated depressions occur in the south-central part of the area. They have a diameter up to 250 metres, and depth up to c. 10 metres (figure 7). These structures are associated with iceberg ploughmarks, and are interpreted as prod marks, resulting from icebergs piercing the seabed.

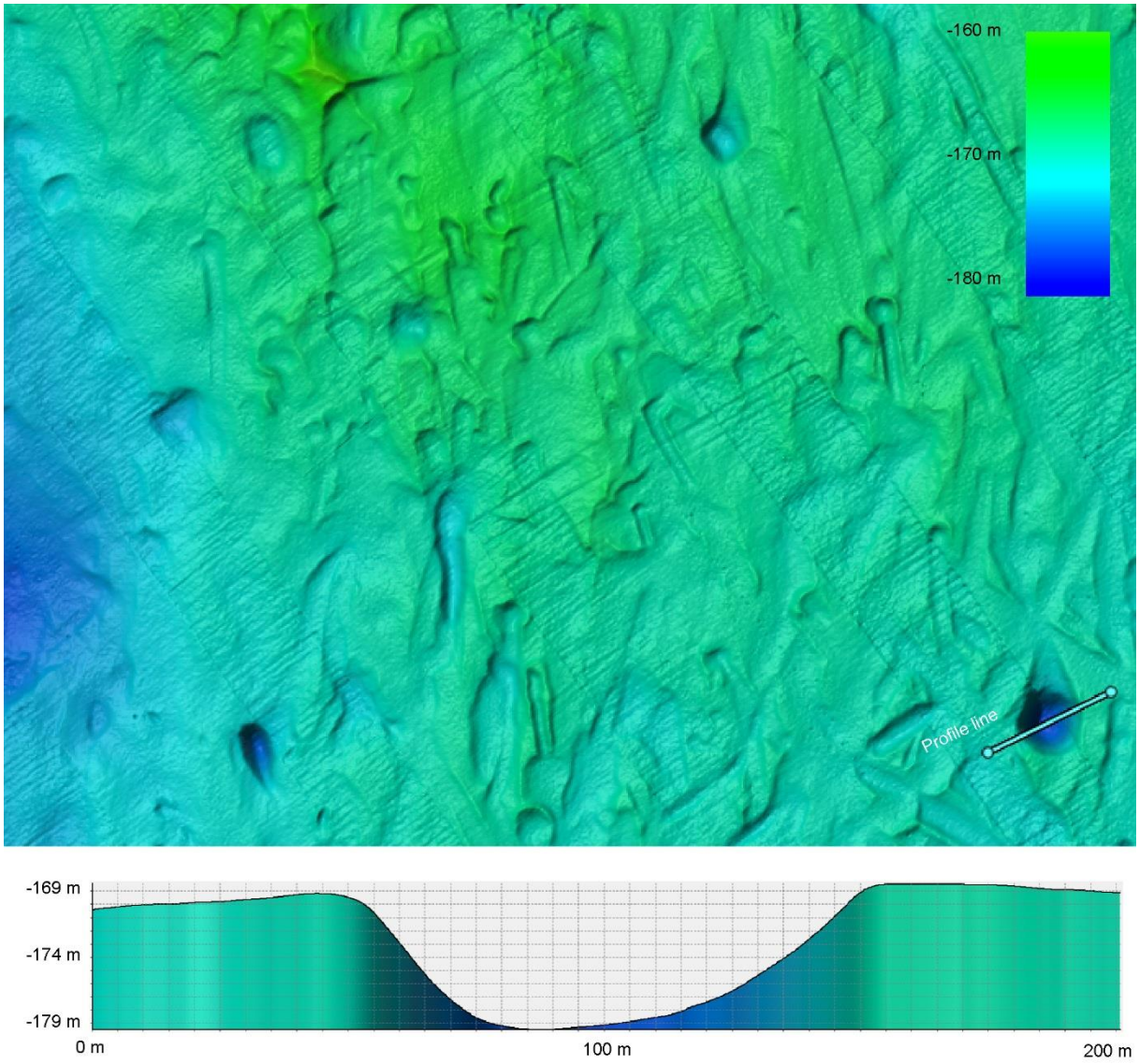

Figure 7. Prod marks caused by iceberg piercing, western part. Lower panel is a profile over the prod mark in the lower right part of the map.

4. RESULTS

In total, 37 gas flares have been identified in the FOSAE-2017-Kvitoya and the FGMG-2018-Kvitoya data sets (table 2). All flares were located in the FOSAE-2017-Kvitoya area, and all except one were located in the westernmost and shallowest part (less than 150 meter) of the area (figure 8).

Table 2. Identified gas flares.

Flare ID	Latitude	Longitude	Depth	Height	Magnitude	Confidence
1308-1	80,55962	33,53430	89	10	2	25
1318-1	80,54876	33,58340	129	29	2	25
1340-1	80,63037	33,48288	94	35	3	25
1340-10	80,62508	33,49216	81	32	3	50
1340-11	80,62499	33,49233	81	32	3	50
1340-12	80,62491	33,49249	81	32	3	50
1340-13	80,62482	33,49266	81	32	3	50
1340-14	80,62474	33,49281	81	32	3	50
1340-15	80,62465	33,49298	81	32	3	50
1340-16	80,62459	33,49311	81	32	3	50
1340-2	80,63012	33,48362	92	57	4	75
1340-3	80,62561	33,49111	81	30	3	50
1340-4	80,62551	33,49128	81	32	3	50
1340-5	80,62542	33,49146	81	33	3	50
1340-6	80,62535	33,49161	81	35	3	50
1340-7	80,62528	33,49173	81	36	3	50
1340-8	80,62523	33,49186	81	35	3	50
1340-9	80,62515	33,49203	81	32	3	50
1345-1	80,61026	33,52056	106	9	3	75
1345-2	80,61010	33,52349	106	17	3	75
1345-3	80,60983	33,52494	105	26	3	75
1345-4	80,60942	33,52614	104	39	4	60
1345-5	80,60932	33,52281	103	40	5	60
1345-6	80,60928	33,52315	102	50	5	60
1345-7	80,60766	33,53934	113	55	2	50
1348-1	80,59365	33,55689	106	76	3	50
1348-2	80,59372	33,55673	107	77	3	50
1348-3	80,59382	33,55670	106	76	3	50
1348-4	80,59565	33,55949	107	77	3	50
1362-1	80,62574	33,54103	102	53	3	60
1363-1	80,56657	33,64212	107	45	3	50
1369-1	80,57619	33,64653	117	105	4	50
1369-2	80,58329	33,64370	117	102	3	25
1373-1	80,57273	33,65301	123	60	4	90
1373-2	80,57263	33,65333	125	34	4	90
1373-3	80,57205	33,65312	126	82	5	90
1465-1	80,66126	34,01406	180	32	2	25

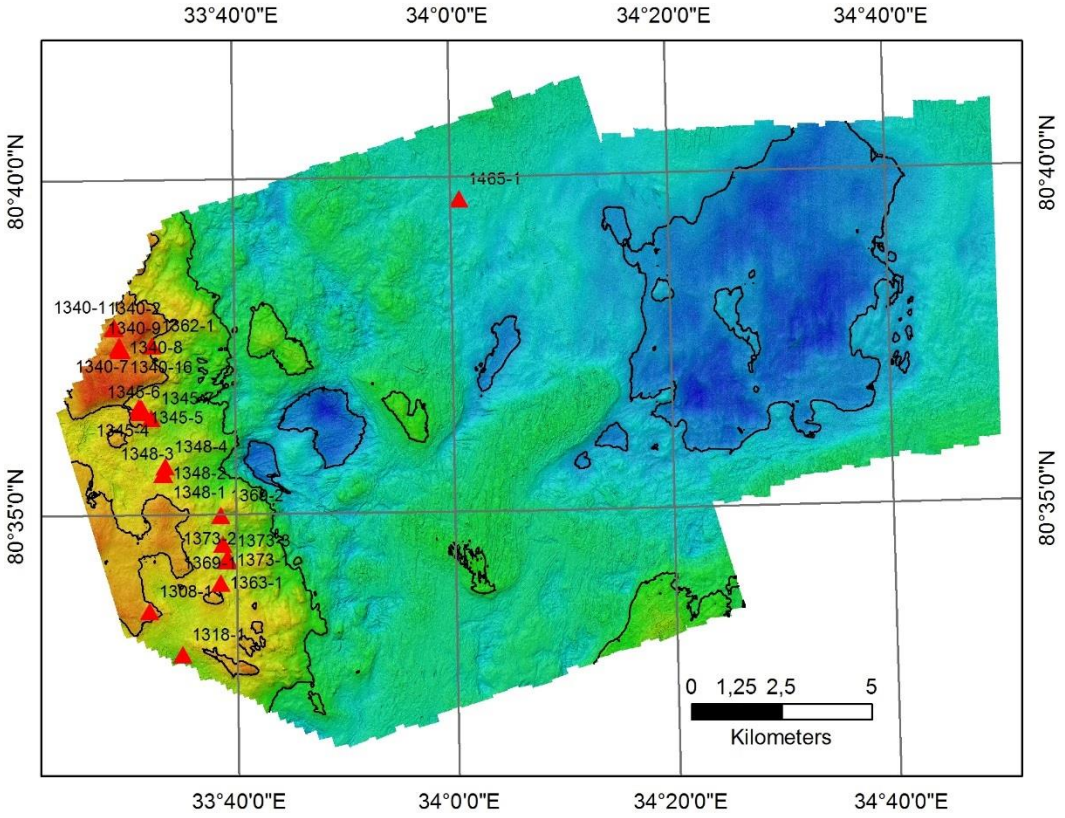

Figure 8. Location of gas flares.

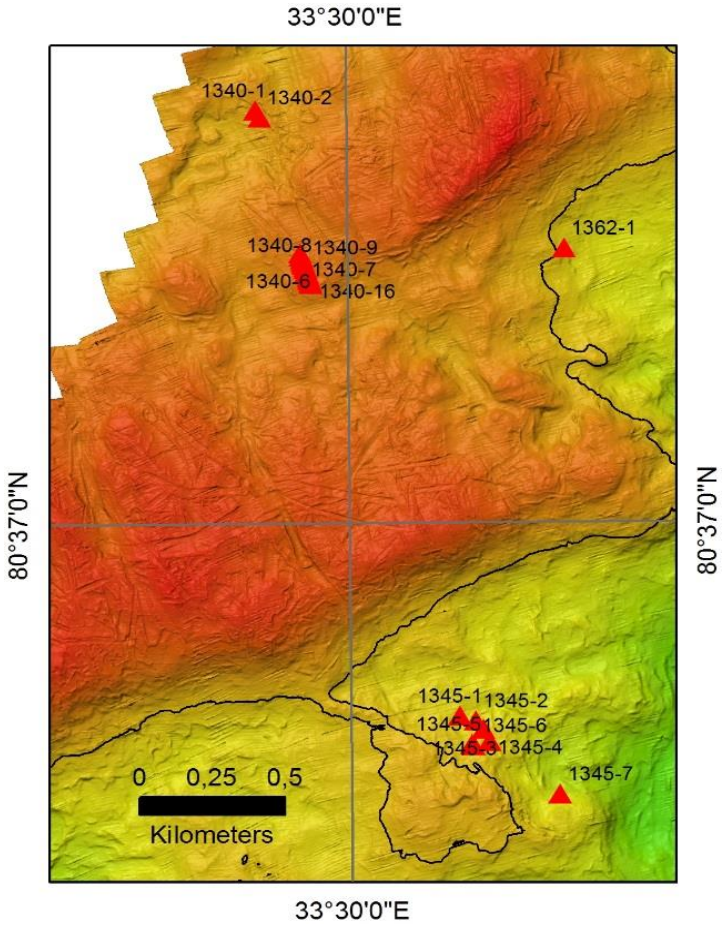

Figure 9. Flares aligned in NNW-SSE direction.

The magnitude of the flares ranges from 2 to 5 – from "weak" to "very strong", and the heights range from c. 10 m to just over 100 metres. Confidence assessments of the flares vary between 25% to 90%. The gas flares tend to be aligned in NNW-SSE direction (figure 9). The gas flares are not associated with backscatter anomalies or topographic features.

The most convincing gas flares are found in line 1373, and range between 34 and 82 metres high, with magnitude 4 to 5 (figure 10). These flares have been assigned a 90% confidence. A 3D view (from Fledermaus) of the flares show that they occur close to the flares in line 1369, and that they are located along the NNE-SSE trend (figure 11). The data can also be visualised directly in Qimera during interpretation, as shown in figure 12.

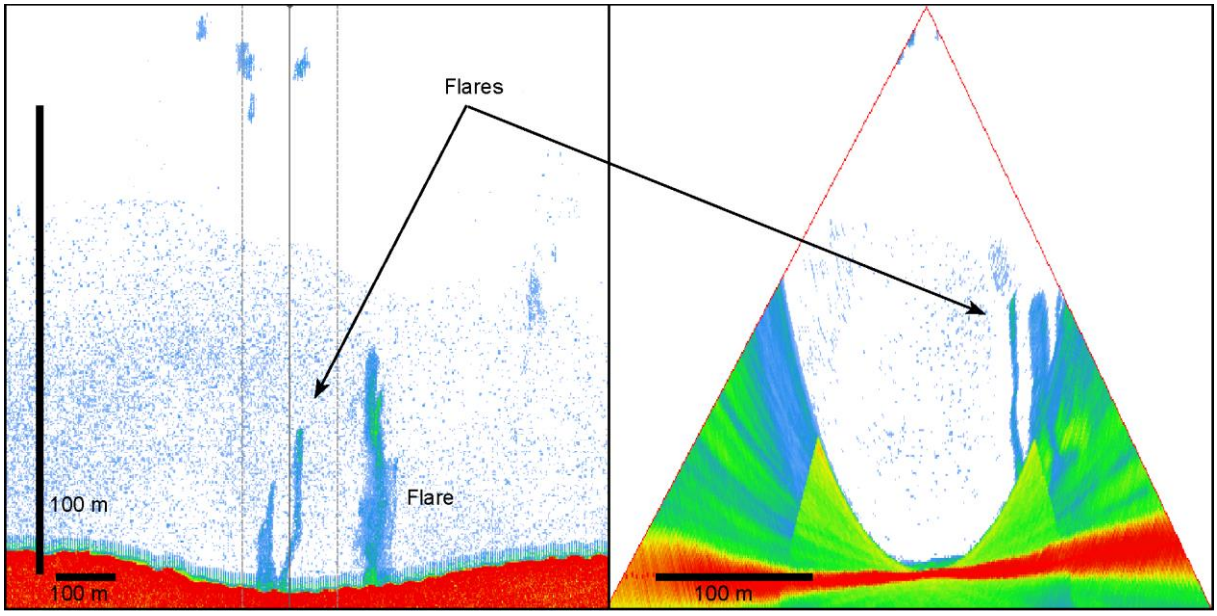

Figure 10. Gas flares in line 1373. Left panel - along-track stacked image showing three gas flares. The three parallel lines show the pings that are stacked in the across-track view. Right panel – across-track stacked image showing two gas flares.

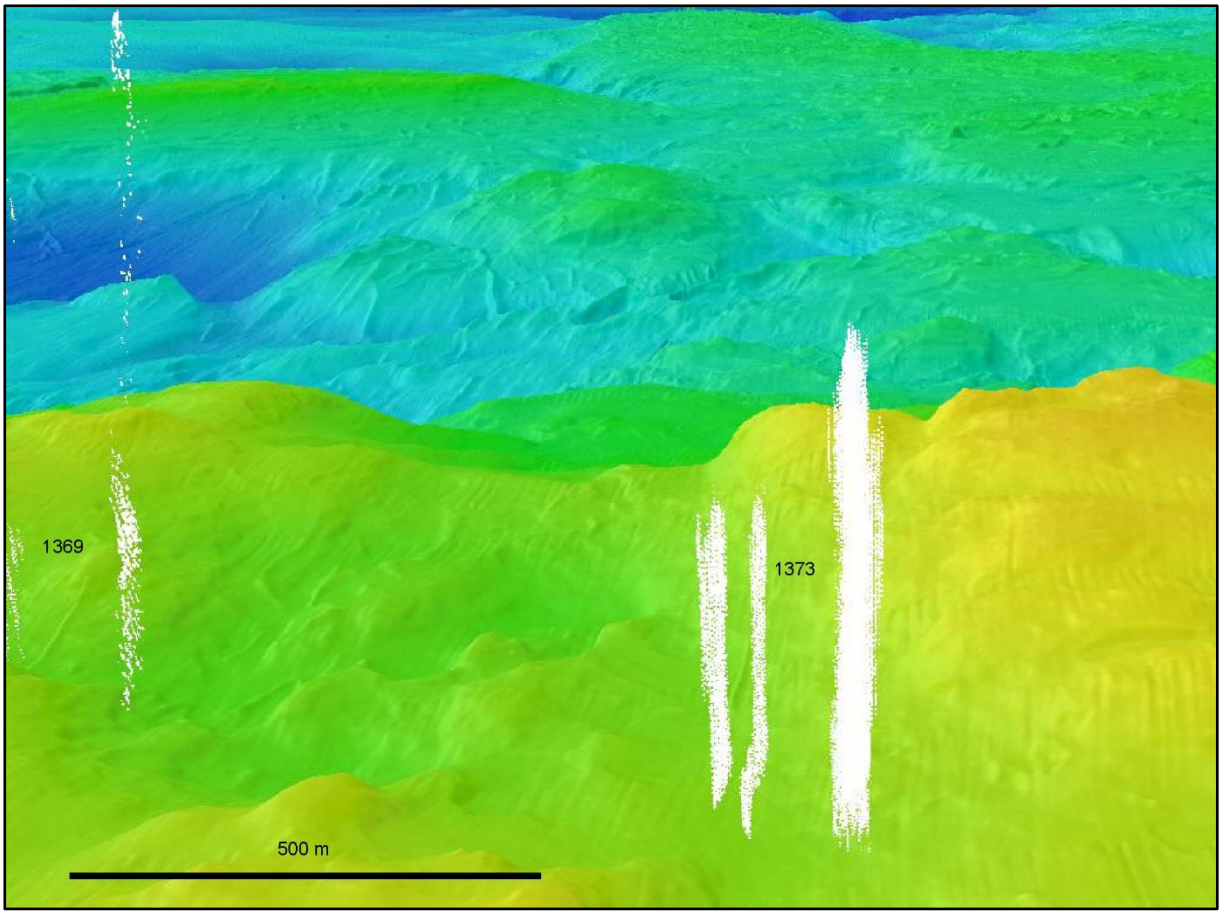

Figure 11. 3D view of the gas flares in line 1373 and line 1369, looking towards ENE. Vertical exaggeration – 5x. The highest 1373 flare is 82 metres.

Another large flare is found in line 1345, in the right part of the left panel in figure 13. Judging from the along-track image (left panel), it appears to be one large flare. However, the right panel indicates that there are at least two flares, forming a composite flare. A closer inspection in Qimera revealed that three separate flares can be seen at the base of this structure. The shape of the flares together with the fact they have three roots indicate that they may be caused by gas. However, the shape is not entirely typical for a gas flare, because the highest intensity and volume of the flare-forming material is found 30-40 metres above the seabed, and it cannot be excluded that they are formed by biological material – possibly fish. They are therefore assigned a 60% confidence. A group of smaller flares is present in the left part of the left panel. These have been assigned a 75% confidence.

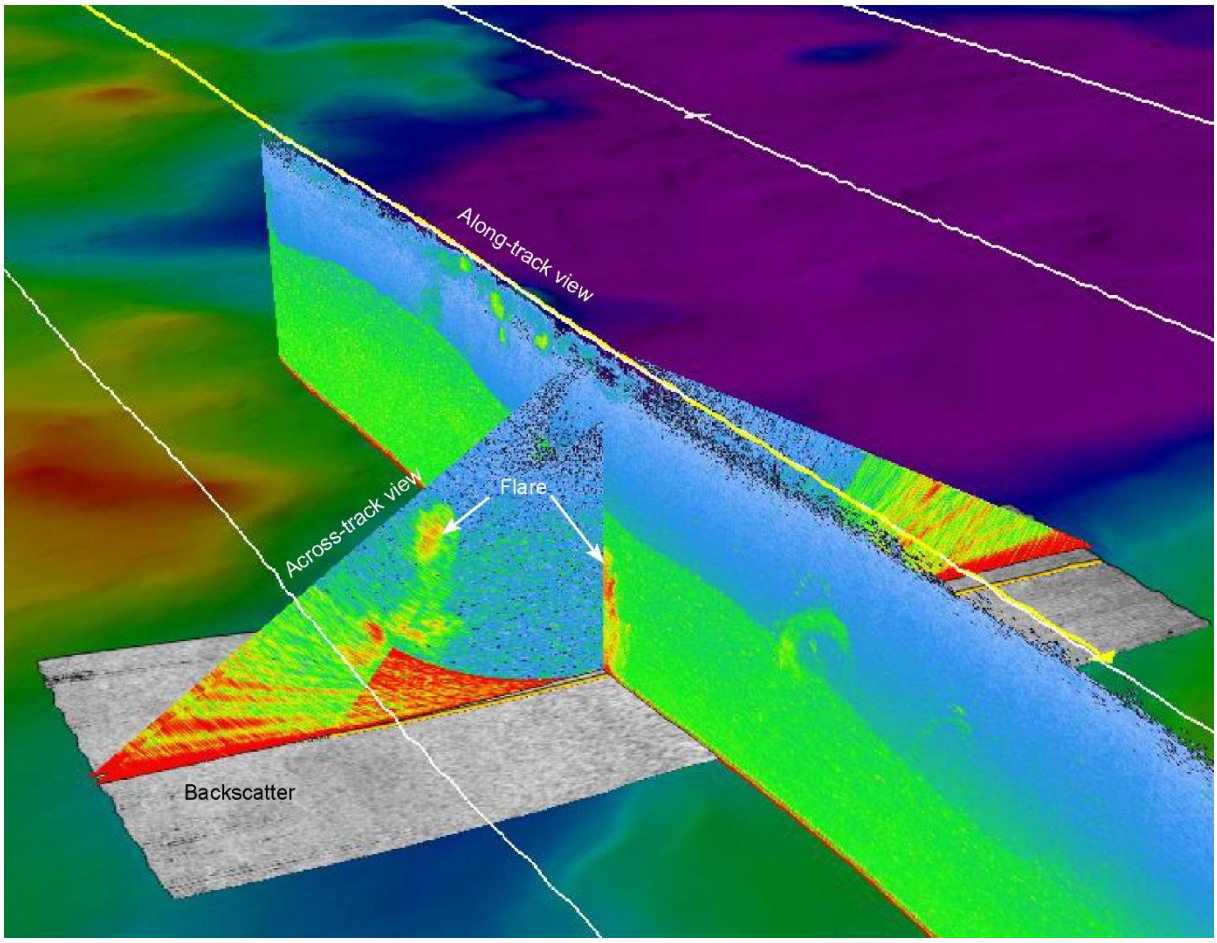

Figure 12. Screen dump from Qimera, showing the flares in line 1373 in simultaneous along- and across-track view. Notice that the same flare can be seen in both the along-track and across-track view. The height of the along-track view is c. 125 m, while the width of the across-track view is c. 395 m.

The along-track stacked image can in some cases give false impressions. Figure 14 (left panel) from line 1362 shows a flare ending in a large, irregular body which will normally be interpreted as biological material. However, the across-track stacked image shows that the flare is separate from the large, irregular body. Consequently, the flare can be interpreted to be a gas flare with reasonable confidence (60%).

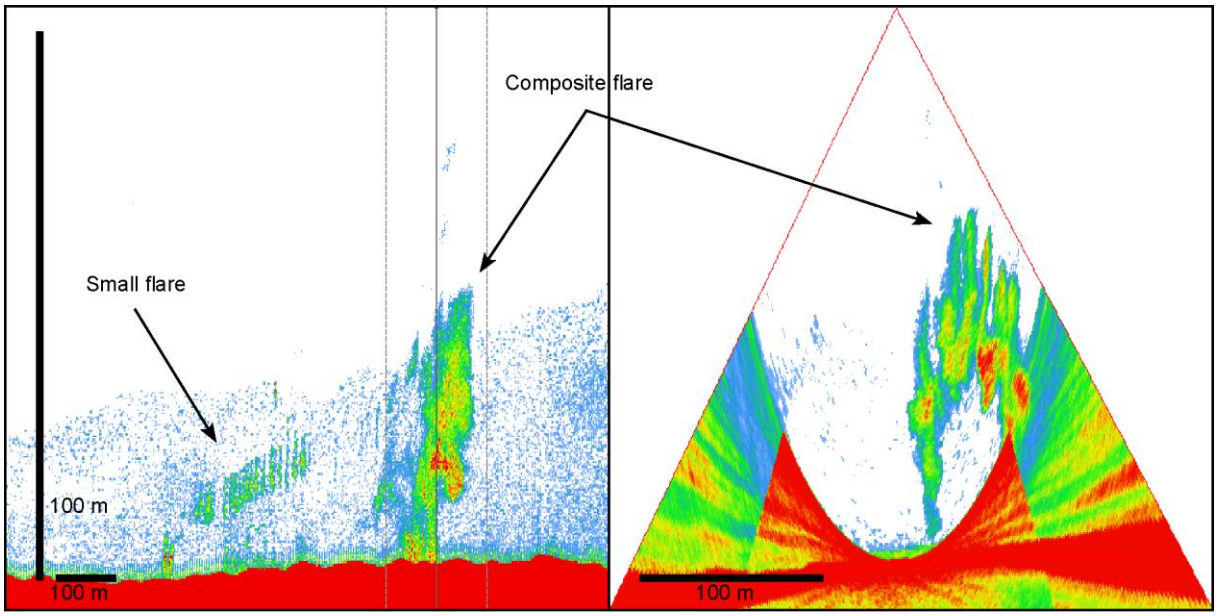

Figure 13. Composite flare in line 1345. Left panel – along-track stacked image. Right panel – across-track stacked image.

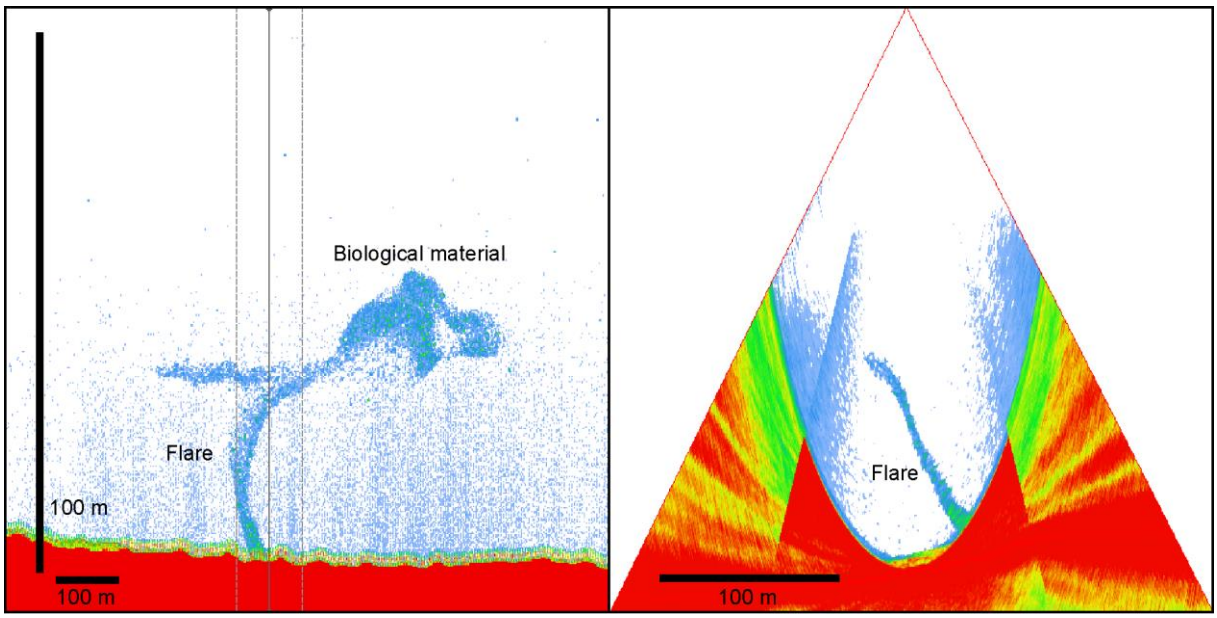

Figure 14. False impression of flare and irregular body of biological material. Left panel – along-track stacked image. Right panel – across-track stacked image. Line 1362.

In some cases, it is indicated that biological material in the water column masks the presence of gas flares. In the left panel of figure 15, all 256 beams have been used to form a stacked along-track image. The result is a dark blue cloud, where very faint vertical structures may be observed. After inspection of the across-track window, it was clear that the acoustic signals defining the vertical structures came from beams 60 to 80. When using only these beams, the vertical structures are much more clearly defined (right panel, figure 15).

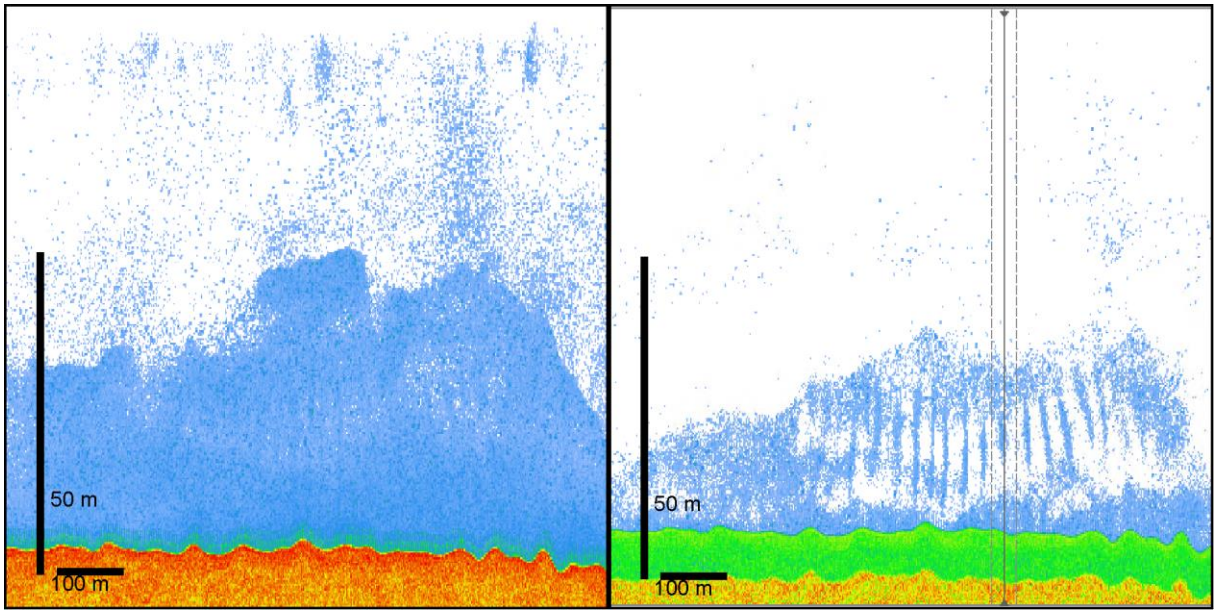

Figure 15. Line 1340 – example of masking of gas flares by biological material. Left panel – all beams were used to construct a stacked along-track image. Right panel – only beams 60 to 80 were used, giving signals mainly from the gas flares.

Many of the lines in the western part are characterised by large amounts of biological material in the water column. This may take several forms – from uniform clouds to intricate cross-cutting structures, to vertical structures resembling gas flares. An example of the latter is shown in figure 16.

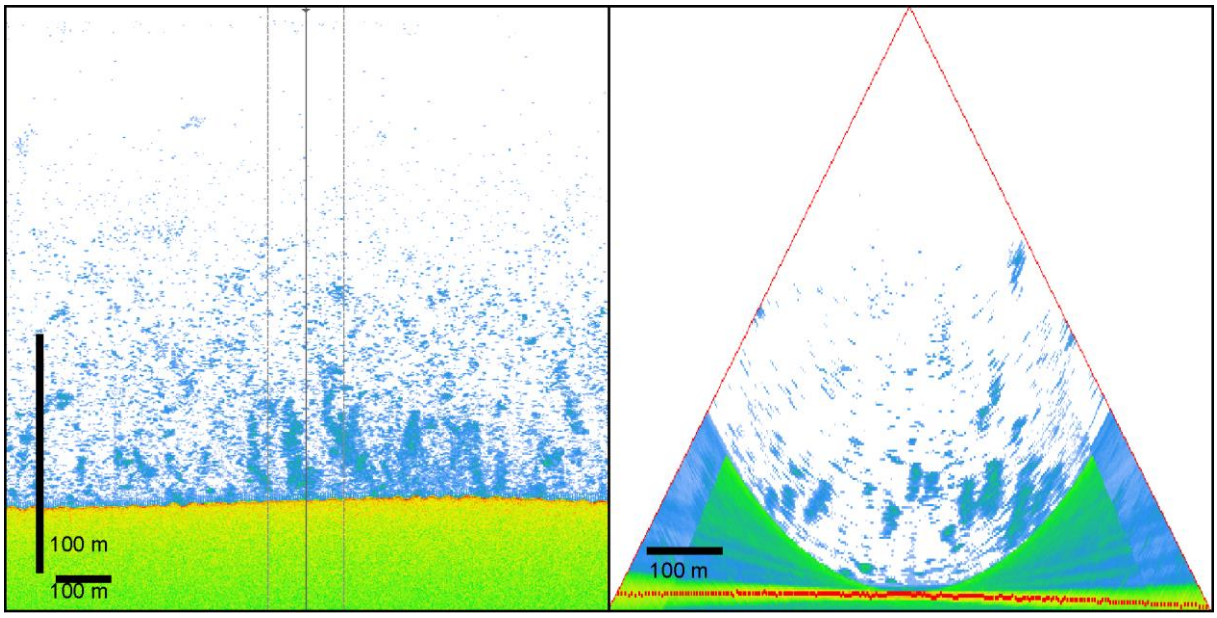

Figure 16. Example of vertical to sub-vertical features in the water column, interpreted to represent biological material. Line 1291.

5. SUMMARY AND CONCLUSIONS

In total, 37 gas flares with varying confidence have been identified in the western part of the study area. Many of them are aligned along a NNW-SSE trend. The alignment of the flares may indicate that their distribution is linked to deep-seated faults, forming pathways for fluids.

Outcropping sedimentary bedrock is indicated in the western depression. The presence of crag and tail structures, and presumably eroded bedding planes indicate that sedimentary bedrock is outcropping here. Low backscatter reflectivity indicates that a thin cover of soft sediments may be expected.

Very few pockmarks have been observed, and those present are small – generally around 50 metres in diameter, and a few metres deep. Even the large depression in the east, with relatively soft sediments, has virtually no pockmarks. This contrasts with many places in the southern and central Barents Sea, where depressions filled with soft sediments may have thousands of pockmarks. No pockmarks were observed associated with the gas flares, but this is not surprising, as the seabed sediment can be expected to be till, judging from the high reflectivity and presence of iceberg plough marks.

Large areas of sand waves in the central northern part of the study area indicate that relatively strong bottom currents occur in this area.

6. REFERENCES

Eiken, O. 1992: An outline of the north western Svalbard continental margin. In: T.O., Vorren et al (eds) Arctic Geology and Petroleum Potential, (Norw. Pet. Soc. Spec Pub 2, 619-629, Elsevier Amsterdam, 619-629.

Elverhøi, A., Lauritzen, Ø. 1984: Bedrock geology of the Northern Barents Sea (West of 35° E) as inferred from the overlying Quaternary deposits. Norsk Polarinstitutt Skrifter, 5-16. Geissler, W.H. & Jokat, W. 2004: A geophysical study of the northern Svalbard continental margin. Geophys. Jour. Int., 158, 50-66.

Hogan, K.A., Dowdeswell, J.A., Noormets, R., Evans, J., O Cofaigh, C. & Jakobsson, M. 2010; Submarine landforms and ice sheet flow in the Kvitøya Trough, north western Barents Sea. Quat. Sci. Rev., 29, 3345-3562.

Lauritzen, Ø. & Ohta, Y. 19984: Geological Map of Svalbard 1:500 000, Sheet 4G, Nordaustlandet, vol. 154D. Norsk Polarintitutt Skrifter.

Leith, T.L., Weiss, H.W., Mørk, A., Århus, N., Elvebakk, G., Embry, A.F., Brooks, P.W., Stewart, K.R., Pchelina, T.M., Bro, E.G., Verba, M.L., Danyushevskaya, A. & Borisov, A.V. 1992: Mesozoic hydrocarbon source-rocks of the Arctic region. In: T.O., Vorren et al (eds) Arctic Geology and Petroleum Potential, (Norw. Pet. Soc. Spec Pub 2, 619-629, Elsevier Amsterdam, 1-25.

Milkov, A.V., Sassen, R., 2003. Two-dimensional modeling of gas hydrate decomposition in the northwestern Gulf of Mexico: significance to global change assessment. Global and planetary Change 36, 31-46.

Ottesen, D., Dowdeswell, J.A. & Rise, L. 2005: Submarine landforms and the reconstruction of fast-flowing ice streams within a large Quaternary ice sheet: the 2500-km long Norwegian-Svalbard margin (57°-80°N). Geol. Soc. Amer. Bull. 117, 1033, http://dx.doi.org.10.1130/B25577.1.

Patton, H., Hubbard, A., Andreassen, K., Winsborrow, M. & Stroeven, A.P. 2016: The build-up, configuration, and dynamical sensitivity of the Eurasian ice-sheet complex to late Weichselian climatic and ocean forcing. Quat. Sci. Rev. 153, 97-121.

Rise, L., Bellec, V.K., Chand, S. & Bøe, R. 2015: Pockmarks in the southwestern Barents Sea and Finnmark fjords. Norw. Jour. Geol. 94, 263-282.

Skarke, A., Ruppel, C., Kodis, M., Brothers, D., and Lobecker, E., 2014, Widespread methane leakage from the sea floor on the northern US Atlantic margin: Nature Geoscience. DOI: 10.1038/NGEO2232

Urban, P., Koser, K. & Greinert, J. 2017. Processing of multibeam water column image data for automated bubble/seep detection and repeated mapping. Limnol. Oceanogr.: Methods 15, 2017, 1-21. Doi: 10.1002/lom3.10138.

GEOLOGICAL
SURVEY OF
NORWAY

· NGU ·

Geological Survey of Norway
PO Box 6315, Sluppen
N-7491 Trondheim, Norway

Visitor address
Leiv Eirikssons vei 39
7040 Trondheim

Tel (+ 47) 73 90 40 00
E-mail ngu@ngu.no
Web www.ngu.no/en-gb/